# Effects of defocus on the transfer function of coherence scanning interferometry

Optics Letters

# Effects of defocus on the transfer function of coherence scanning interferometry

Rong Su,[1,*] Matthew Thomas,[1] Richard Leach,[1] and Jeremy Coupland[2]

[1]Manufacturing Metrology Team, Faculty of Engineering, University of Nottingham, University Park, Nottingham NG7 2RD, UK
[2]Wolfson School of Mechanical, Electrical and Manufacturing Engineering, Loughborough University, Loughborough LE11 3TU, UK
*Corresponding author: rong.su@nottingham.ac.uk

Received 17 August 2017; revised 21 October 2017; accepted 6 November 2017; posted 7 November 2017 (Doc. ID 304940); published 21 December 2017

**Coherence scanning interferometry (CSI) offers three-dimensional (3D) measurement of surface topography with high precision and accuracy. Defocus within the interferometric objective lens, however, is commonly present in CSI measurements and reduces both the resolving power of the imaging system and the ability to measure tilted surfaces. This Letter extends the linear theory of CSI to consider the effects of defocus on the 3D transfer function and the point spread function in an otherwise ideal CSI instrument. The results are compared with measurements of these functions in a real instrument. This work provides further evidence for the validity of the linear systems theory of CSI.**



***OCIS codes:*** (180.0180) Microscopy; (120.3180) Interferometry; (120.3940) Metrology; (110.0110) Imaging systems; (150.1488) Calibration; (220.1010) Aberrations (global).

https://doi.org/10.1364/OL.43.000082

In two-dimensional imaging systems, such as those used in wide-field microscopy, the effects of defocus generally degrade image quality, although in certain circumstances one or more defocused images have been used as a means of edge enhancement [1] and to retrieve phase information from intensity images [2]. The effect of defocus in three-dimensional (3D) imaging instruments, such as confocal microscopy, is more complex and depends on the relative focus of the illumination and observation optics, such that markedly different responses are observed for the reflection and transmission imaging modes [3]. In this Letter we consider the effect of defocus on the performance of the interference microscopes that form the basis of the measuring technique known as coherence scanning interferometry (CSI). Reference [4] shows how easily defocus causes measurement errors in CSI. In a way that is analogous to confocal microscopy, it is the relative defocus between the object and reference arms that is important in this case, and the effect of defocus on the transfer function (TF) and point spread function (PSF) that characterize the 3D performance in CSI is determined.

CSI is a well-established technique for 3D measurement of surface topography with high precision and accuracy [5]. When using CSI to measure the surface topography of an object, either the object or objective lens is scanned axially to generate an image stack that contains interference fringes, from which the surface topography is reconstructed. Two of the most common interferometric objectives used in CSI are those of Michelson and Mirau design (Fig. 1). Michelson objectives are mostly used for low numerical aperture (NA), low-magnification systems (10× and lower) while Mirau objectives are more useful at higher NA and higher magnification (10× to 100×). In addition, Linnik objectives are often used for high-magnification systems, when a larger working distance than with a Mirau objective is desired [6,7].

If the reference mirror of the interferometer is positioned at the focal plane of the lens, the sharpest image is obtained exactly when the optical path difference (OPD) between the two arms of the interferometer is zero, where the modulation envelope of the low-coherence interference signal is at its peak. In a Mirau objective, the reference mirror is a surface conjugate to the best focus plane of the object [7]. In this case, the surface topography can be reconstructed from the fringes with the optimal lateral resolution.

Defocus in CSI means that the reference mirror is not accurately positioned at the conjugate focal plane of the lens,

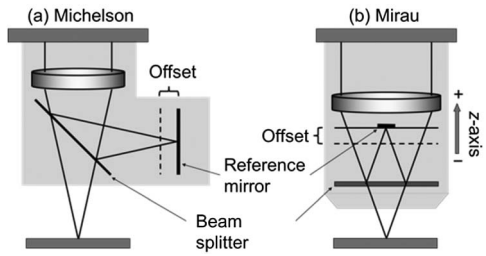


**Fig. 1.** Common interferometers in CSI: (a) Michelson and (b) Mirau type.

as illustrated by the dashed line in Fig. 1. Consequently, the peak position of the coherence envelope of the fringes will be shifted away from where the sharpest intensity image of the surface is obtained. In other words, there is an offset between the interferometric focus and the microscopic focus, where the former is determined by the OPD and the latter is determined by the position of the focal plane of the lens, in a similar manner to that of an ordinary microscope. In this study, a ZYGO NewView 8300 system with 50× Mirau objective (0.55 NA) is used. The position of the beam splitter can be adjusted along the optical axis in order to place the reference mirror into focus [Fig. 1(b)]; nevertheless a perfect mechanical adjustment is difficult to achieve, particularly for Linnik objectives [8].

The common method for evaluating the degree of defocus is conducted in the spatial domain by imaging a planar surface with features, and the sharpest image of the surface is expected when the fringes are brightest or darkest. For example, a rectangular grating with sharp edges or a slightly roughened optical flat can be used. As shown in Fig. 2, the axial offset between the microscopic and interferometric signals can be observed in the cross-sectional views of the 3D CSI images of a roughened optical flat. The intensity variation in the background of the fringes can be considered as the microscopic image of the surface, i.e., the convolution between the 3D microscopic PSF and the object function [9]. The small particulates in the surface may form the dark and spindle-shaped artefacts in the cross-sectional images. Thus, the central position of the "spindle" (in the axial direction) can be used for estimation of the focal plane of the lens. The estimated axial offsets between the interferometric focus and the microscopic focus are −2.4 μm, −1.3 μm, −0.1 μm, 1.5 μm, and 3.3 μm, for Figs. 2(b)–2(f), respectively. The measurements were done by adjusting the position of the beam splitter by manually rotating the outer casing of the objective lens.

In this study, we will present a new method to analyze the defocus condition of a CSI system by examining the 3D TF of the system in the spatial frequency domain, and the effects of defocus on the TF will be investigated. The advantage of this approach is that a CSI system can be effectively characterized by its TF, including the spatial bandwidth, resolution, and optical aberrations in the system [10,11].

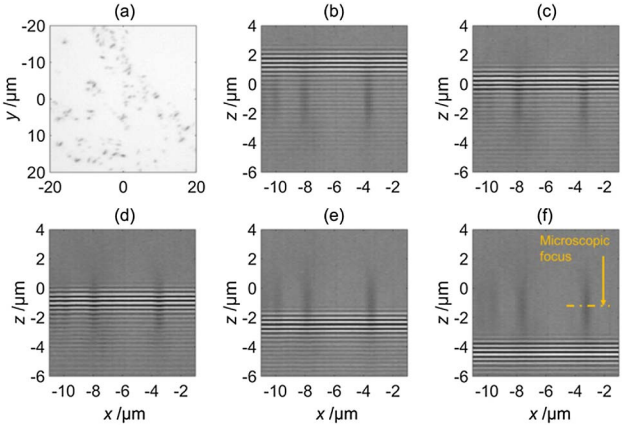


**Fig. 2.** (a) Intensity image of the roughened optical flat in the $x-y$ plane and cross-sectional CSI images of the surface taken at different focus conditions. The estimated axial offsets are (b) −2.4 μm, (c) −1.3 μm, (d) −0.1 μm, (e) 1.5 μm, and (f) 3.3 μm. (Direction is defined in Fig. 1.)

Recent studies show that CSI measurement of a surface can be considered as a linear filtering operation if the Kirchhoff approximation is made, such that multiple scattering from the surface is negligible. This assumption requires the surface to be slowly varying on the optical scale, i.e., the local radius of curvature is much larger than the wavelength [12]. The detailed derivation of the linear theory of surface measurement by CSI can be found elsewhere [10,13]. The linear systems theory shows that the interference term of the CSI signals in the spatial frequency domain ($k$-space), $I(\boldsymbol{k})$, can be expressed as the multiplication of the object spectrum, $O(\boldsymbol{k})$, and the TF (also understood as the linear shift-invariant filter), $H(\boldsymbol{k})$, as

$$I(\boldsymbol{k}) = O(\boldsymbol{k})H(\boldsymbol{k}), \tag{1}$$

where $O(\boldsymbol{k})$ is the Fourier transform of the object function, defined by the optical property and topography of the surface [13],

$$o(x, y, z) = 4\pi jRw(x, y)\delta[z - s(x, y)], \tag{2}$$

where $j = \sqrt{-1}$, $R$ is the Fresnel amplitude reflection coefficient, and $w(x, y)$ is a window function with smooth cutoff for making the object function space-limited. The object is defined as an infinitely thin foil by the Dirac delta function $\delta(z)$ based on the surface topography $s(x, y)$ (this is referred to as the "foil model" of the surface in other publications). Using the foil model, if the object function is known, then the TF can be easily retrieved. It has been shown that a precision sphere which has uniformly distributed surface slopes can be used for calibration of the TF [14,15], where the diameter of the sphere should be much greater than a wavelength and smaller than the field of view.

Based on the linear theory, the theoretical TF of CSI can be calculated given the spectrum of the light source and NA of the system. We first consider the 3D TF of an optical system that operates at the wavenumber $k_0 = 1/\lambda$ ($\lambda$ is the illumination wavelength) and is restricted by a finite NA ($N_A$) given by [13]

$$G(\boldsymbol{k}, k_0) = \frac{j}{4\pi k_0^2}\delta(|\boldsymbol{k}| - k_0)\text{step}\left(\frac{\boldsymbol{k}\cdot\hat{\boldsymbol{z}}}{|\boldsymbol{k}|} - \sqrt{1 - N_A^2}\right). \tag{3}$$

The TF of an optical system is a spherical shell in $k$-space truncated by the Heaviside step function that is determined by the NA [Fig. 3(a)]. The spherical shell is referred to as the Ewald sphere and its radius is $k_0$ [10,16]. In the spatial domain, the 3D impulse response, i.e., PSF, of the optical system is obtained as the inverse Fourier transform of the TF as $g(\boldsymbol{r}, k_0) = \mathcal{F}^{-1}\{G(\boldsymbol{k}, k_0)\}$.

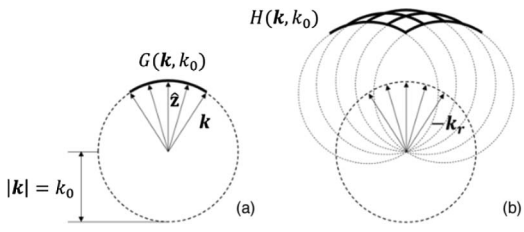


**Fig. 3.** Cross-sectional views of (a) the TF of an optical system with a finite NA and (b) the TF of CSI (monochromatic illumination is assumed).

According to Coupland *et al.* [13], the TF of CSI is given by the convolution of $G(\boldsymbol{k}, k_0)$ with itself [see Fig. 3(b)] and integrated over the entire spectrum of the light source, $S(k_0)$, as

$$H(\boldsymbol{k}) = \left(\frac{|\boldsymbol{k}|^2}{2\boldsymbol{k}\cdot\hat{\mathbf{z}}}\right) \times \iint G(\boldsymbol{k}_r, k_0)G(\boldsymbol{k}-\boldsymbol{k}_r, k_0)d^3k_r S(k_0)\mathrm{d}k_0, \quad (4)$$

where $\boldsymbol{k}_r$ is the wave vector of the reference light and $\hat{\mathbf{z}}$ is a unit vector in the direction of the optical axis. According to Eq. (1), the imaging process can be considered as a linear filtering operation that modifies the object spectrum by selecting only the spatial frequency components that lie within the passband defined by $H(\boldsymbol{k})$.

Defocus in CSI appears when there is an offset, $\delta z$, of the reference mirror along the optical axis, which is equivalent to introducing a linear shift to the impulse response of the reference beam. The PSF is, therefore, modified as $g(\boldsymbol{r}+2\delta z\cdot\hat{\mathbf{z}}, k_0)$, where the factor "2" comes from the fact that the OPD is doubled by the reflection of the reference beam. Using the shift property of the Fourier transform and taking the inverse Fourier transform of the modified PSF, we obtain the TF of the optics of the reference arm as $G(\boldsymbol{k}, k_0)\exp(j4\pi\boldsymbol{k}\delta z\cdot\hat{\mathbf{z}})$, where the additional exponential term indicates a phase shift determined by $2\delta z$. By replacing one of the $G(\boldsymbol{k}, k_0)$ terms in Eq. (4), we obtain a more general expression for the TF of a CSI system, taking account of defocus:

$$H_d(\boldsymbol{k}) = \left(\frac{|\boldsymbol{k}|^2}{2\boldsymbol{k}\cdot\hat{\mathbf{z}}}\right)\iint G(\boldsymbol{k}_r, k_0)\exp(j4\pi\boldsymbol{k}_r\delta z\cdot\hat{\mathbf{z}}) \times G(\boldsymbol{k}-\boldsymbol{k}_r, k_0)d^3k_r S(k_0)\mathrm{d}k_0. \quad (5)$$

It is noted that a special case occurs when the reference mirror is in focus, i.e., $\delta z = 0$. Based on Eq. (5), the theoretical TF of the CSI system used in this study can be calculated. A Gaussian spectrum of the illumination source is assumed, and based on the specification of the instrument, the central wavelength is 0.58 μm and the bandwidth (full width at half-maximum) is 0.8 μm. As shown in Fig. 4, the TFs are calculated at different defocus conditions, and the corresponding PSFs are obtained by taking the inverse Fourier transform of the TFs. As shown in Fig. 4, the spatial bandwidth of the CSI, determined by the magnitude of the TF, reduces with the increasing offset of the reference mirror from the focused position. This reduction is particularly noticeable in the lateral direction of $k$-space. Therefore, the high spatial frequency components of the object spectrum, corresponding to high surface slopes and fine structures, cannot be fully recorded and reconstructed. The reduction of the bandwidth also causes the broadening effect of the PSF.

The phase terms of the TFs are shown in the second column of Fig. 4. For visualization purposes, 3D windows determined by 1% of the magnitudes of the TFs are applied to the respective phase plots, displaying only the phase terms within each passband, i.e., the phase terms in the irrelevant regions in $k$-space are not plotted. Horizontal fringes are observed in the phase terms when defocus is present, and the spacing frequency of these fringes is proportional to the amount of offset. The horizontal fringes also indicate that the phase term is not dependent on the lateral spatial frequency components, i.e., defocus is an axial aberration.

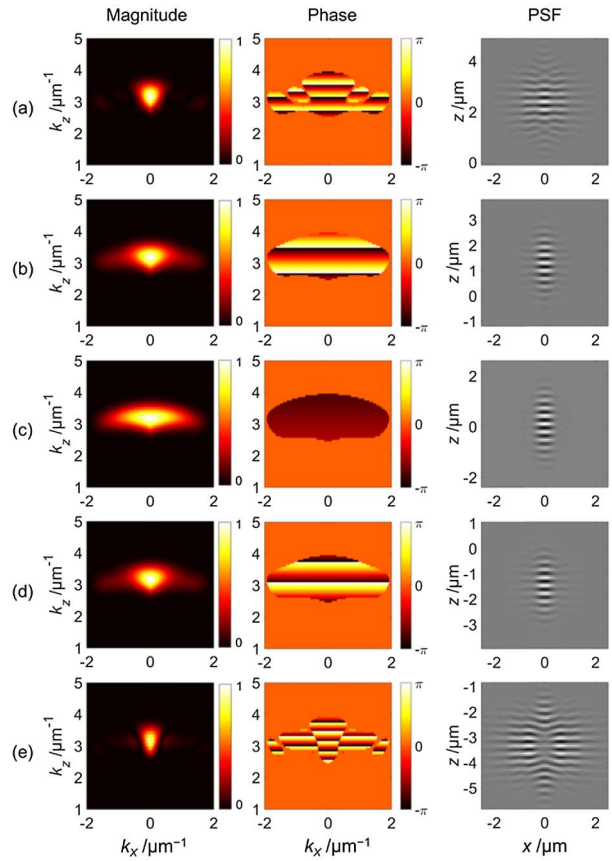


**Fig. 4.** Cross-sectional views of the theoretical TFs and PSFs of CSI at different focus conditions: (a) −2.4 μm, (b) −1.3 μm, (c) −0.1 μm, (d) 1.5 μm, and (e) 3.3 μm. Note the change in $z$-axis of the PSF plot.

As we know that height measurement in CSI is dependent on the phase of the recorded fringes, it follows that a non-uniform phase term in the TF will shift and distort the recorded fringes and correspondingly change the height measurement result. As a consequence, the axial position of the PSF is shifted in the presence of defocus, and this shift explains the offset between the interferometric focus and the microscopic focus (Fig. 2). Moreover, changes in the magnitude of the TF mean that we should expect loss of signal and tilt dependent errors due to defocus.

In general, the effects of defocus on the TFs and PSFs are identical for positive and negative offsets ($\delta z$ larger or smaller than zero) except for the changes in the signs of the gradient of the phase terms, corresponding to the PSFs being shifted downwards and upwards along the optical axis.

As discussed before, the TF of CSI can also be measured experimentally using a precision sphere, and in this case a sphere with a diameter of 36.6 μm is used. The detailed procedure of the calibration can be found elsewhere [14,15]. The CSI image stacks of the sphere are acquired at the same focus conditions as those shown in Fig. 2. The acquired CSI images and the measured height maps near the top of the spherical cap are shown in Fig. 5. The contrast of the fringes decreases and

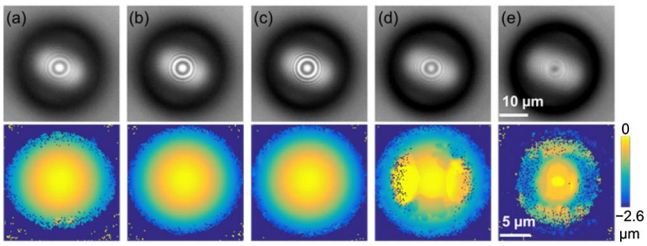


**Fig. 5.** Top-view CSI images of the spherical cap at different focus conditions (top row) and the corresponding height maps (bottom row): (a) −2.4 μm, (b) −1.3 μm, (c) −0.1 μm, (d) 1.5 μm, and (e) 3.3 μm.

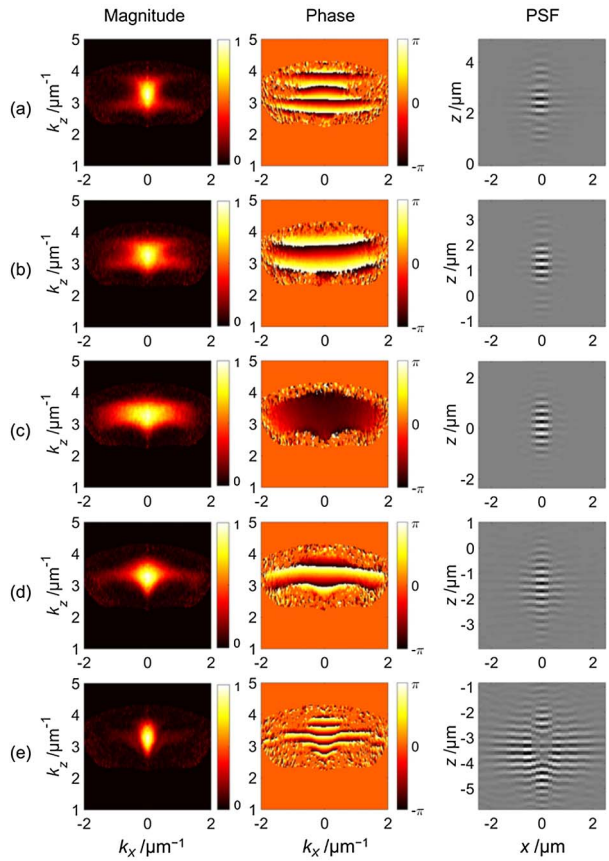


**Fig. 6.** Measured TFs and derived PSFs at different focus conditions: (a) −2.4 μm, (b) −1.3 μm, (c) −0.1 μm, (d) 1.5 μm, and (e) 3.3 μm.

the measurement error increases as the amount of defocus becomes larger. For an ideal CSI system with NA 0.55, the maximum detectable slope angle is approximately 30° on the smooth spherical cap.

The measured TFs and the derived PSFs of the CSI system are shown in Fig. 6. We assume that the axial position of the sphere was not changed in the instrument's coordinate system because the sphere was not moved during the measurements. In general, the experimental results agree with the theoretically calculated TFs, although some discrepancies are observed in both the magnitudes and phase terms of the TFs. Comparing Fig. 6 with Fig. 4, the magnitudes of the TFs are unbalanced for the positive and negative offsets of the reference mirror of the interferometry, and the horizontal fringes in the phase terms are not as straight as predicted in the simulated results. The discrepancies indicate the presence of other optical aberrations that are dependent on lateral frequency components, e.g., spherical aberration, as is clearly seen in the phase term of Fig. 6(c).

In summary, the fringe generation in CSI in the presence of defocus is analyzed based on the linear systems theory of surface measurement. We demonstrate that defocus in CSI can be revealed and evaluated in the spatial frequency domain by measuring the TF of the system using a precision sphere. The advantage is that the TF provides information on the spatial bandwidth (characterized by its magnitude part) and optical aberration (characterized by its phase term) in the system. Moreover, the resolution and PSF of the system may also be derived from the TF. In the presence of defocus, the lateral resolution of the system and the fringe contrast of high surface slopes are degraded because of the reduction of spatial bandwidth and broadening of the PSF. The unbalanced magnitudes of the TFs and the lateral dependencies of the phase terms indicate the presence of other aberrations, e.g., spherical aberration, and will be addressed in our continued research. In addition, this study provides further experimental evidence for the validity of the linear systems theory of surface measurement by CSI.

**Funding.** This work was supported by the Engineering and Physical Sciences Research Council (EPSRC) (EP/M008983/1); European Metrology Programme for Innovation and Research (EMPIR) project FreeFORM (15SIB01).

## REFERENCES

1. C. J. R. Sheppard and D. K. Hamilton, Opt. Acta **31**, 723 (1984).
2. R. M. von Bunau, H. Fukuda, and T. Terasawa, Jpn. J. Appl. Phys. **36**, 7494 (1997).
3. M. Gu and C. J. R. Sheppard, Appl. Opt. **31**, 2541 (1992).
4. J. Petzing, J. M. Coupland, and R. K. Leach, in *NPL Measurement Good Practice Guide No. 116* (2010), p. 59.
5. P. de Groot, in *Optical Measurement of Surface Topography*, R. K. Leach, ed. (Springer, 2011), p. 187.
6. P. de Groot, Adv. Opt. Photon. **7**, 1 (2015).
7. J. Schmit, K. Creath, and J. C. Wyant, in *Optical Shop Testing*, D. Malacara, ed. (Wiley, 2007), p. 667.
8. J. Dong, R. Lu, Y. Li, and K. Wu, Appl. Opt. **50**, 5861 (2011).
9. N. Nikolaev, J. Petzing, and J. M. Coupland, Appl. Opt. **55**, 3555 (2016).
10. J. M. Coupland and J. Lobera, Meas. Sci. Technol. **19**, 07010 (2008).
11. M. R. Foreman, C. L. Giusca, J. M. Coupland, P. Török, and R. K. Leach, Meas. Sci. Technol. **24**, 052001 (2013).
12. P. Beckmann and A. Spizzichino, *The Scattering of Electromagnetic Waves from Rough Surfaces* (Pergamon, 1963).
13. J. M. Coupland, R. Mandal, K. Palodhi, and R. K. Leach, Appl. Opt. **52**, 3662 (2013).
14. R. Mandal, J. M. Coupland, R. K. Leach, and D. Mansfield, Appl. Opt. **53**, 1554 (2014).
15. R. Su, Y. Wang, J. M. Coupland, and R. K. Leach, Opt. Express **25**, 3297 (2017).
16. C. J. R. Sheppard and C. J. Cogswell, J. Microsc. **159**, 179 (1990).